Microchimica Acta (2020) 187:544
https://doi.org/10.1007/s00604-020-04530-1

ORIGINAL PAPER

Porous PtAg nanoshells/reduced graphene oxide based biosensors for low-potential detection of NADH

Hongxiao Yang[1] · Jiagang Hou[2] · Zhaohui Wang[1] · Qiuxia Zhou[1] · Caixia Xu[1]

Received: 3 January 2020 / Accepted: 22 August 2020

Abstract

A superior NADH sensing platform was constructed based on porous PtAg nanoshells supported on reduced graphene oxide (PtAg/rGO) in the absence of any enzymes and redox mediators. The PtAg/rGO composite was prepared via one-step reduction combined with galvanic replacement reaction. The as-made PtAg/rGO assembles multiple structural advantages of coherent conductive matrix, rich electroactive sites, and high specific surface area, accompanied by the unique alloying effect. The PtAg/rGO possesses adequate active reaction sites and fluent electron transport pathway towards the electrocatalytic NADH oxidation, thus presenting significantly increased oxidation current and negative shift of 330 mV in applied potential relative to the bare GCE. By virtues of the outstanding electrocatalytic activity, PtAg/rGO exhibits effective amperometric detection of NADH at 0.15 V within a wide linear concentration range of 2–2378 μM, a high sensitivity of 92.62 μA mM^{-1} cm^{-2}, low detection limit of 0.2 μM, and long-term detection over 2500 s. Moreover, the as-constructed biosensors can achieve accurate NADH detection in human serum samples, indicating its promising application feasibility in fundamental and clinic research.

Keywords Platinum-silver · Nanocomposite · Electrocatalyst · Electrochemical sensing

Introduction

As an important coenzyme in the human body, NADH participates in hundreds of enzymatic reactions concerning over 300 dehydrogenases. The precise, convenient, and fast NADH quantification has attracted increasing research interests. Recently, the electrochemical method has been wildly developed for NADH detection, benefiting from the high accuracy, outstanding sensitivity, rapid response, good portability, as well as convenient operation [1, 2]. However, the electrochemical quantification of NADH possesses several inherent weaknesses. The direct electron transfer of NADH at bare electrode is kinetically sluggish, highly irreversible, and accompanied by requiring large activation energy and high applied potentials [3]. Moreover, the electrochemical NADH oxidation is usually associated with side reactions due to the required high overpotential [4]. The high overpotential and production of the by-product lead to the rapid surface passivation of electrode owing to the adsorption of intermediates and oxidation products. Until now, the electrochemical quantification of NADH faces two prominent challenges to realize the practical application. The decrease of the overpotential for NADH oxidation and the optimization of the electron transfer during the electrochemical reaction are the first challenges to be solved. The secondary challenge is the achievement of excellent selectivity and long-term stability for the application in real samples.

Considerable efforts have been devoted to reduce the high overpotential by improving the electron-transfer kinetics of NADH oxidation [5]. The modification of electrodes with appropriate electrocatalysts can accelerate the electron transport and enhance the efficiency of the NADH electrocatalytic

Electronic supplementary material The online version of this article (https://doi.org/10.1007/s00604-020-04530-1) contains supplementary material, which is available to authorized users.

✉ Caixia Xu
chm_xucx@ujn.edu.cn

[1] Institute for Advanced Interdisciplinary Research (iAIR), School of Chemistry and Chemical Engineering, Collaborative Innovation Center of Technology and Equipment for Biological Diagnosis and Therapy in Universities of Shandong, University of Jinan, Jinan 250022, Shandong Province, China

[2] Qilu University of Technology (Shandong Academy of Sciences), Jinan 250353, Shandong Province, China

oxidation [6]. With the rapid development of nanotechnology, mounting nanomaterials were designed and applied as the electrocatalysts for NADH detection. Platinum-based nanomaterials have been deemed as remarkable electrocatalysts with the intrinsic advantages of fast electron transfer, impressive electrochemical stability, and excellent biocompatibility [7]. But the monocomponent Pt is especially sensitive to the fouling from absorbed intermediates in the NADH oxidation reaction. The strategy of alloying Pt with other transition metals is regarded as an effective tactic to optimize its electrocatalytic performances, which can prevent the adsorption of the intermediates species on Pt atoms by forming adsorbents on the secondary metal atoms [8, 9]. Among the transition metals, Ag is specially considered as excellent candidate because of its favorable electronic structure [10] and specific anti-poisoning property in some electrooxidation process [9]. Especially, Ag presents similar lattice constant to Pt, which benefits the rational arrangement of hetero-atoms in PtAg alloy [11]. The synergistic effect between hetero-atoms in PtAg alloy can improve the geometric and electronic structure of the electrocatalysts, activating the surface active sites as well as further meliorating the catalytic performance [8]. Xu et al. prepared the supported hollow PtAg nanodendrites with high performance for electrooxidation of formic acid [8]. The synergistic effects between Pt and Ag play a crucial role in the dramatic performance improvement.

In view of improving the electrooxidation kinetics of NADH, the conductive catalyst supports is supposed to be another efficient approach to facilitate the electron transfer and catalytic durability of Pt-based catalysts. As a two-dimensional carbon crystal with one atom thickness, reduced graphene oxide (rGO) represents a typical class of ideal hosting substrates with an extraordinary π-conjugated structure [7, 12, 13], which features various attractive merits including superior electrical conductivity, strong affinity, large surface area, and high stability [14]. Govindhan reported the highly sensitive NADH detection based on the Au nanoparticles/rGO nanocomposite [15]. Compared with Au nanoparticles, the Au nanoparticles/rGO biosensor presented much higher catalytic current density and lower working potential. Roushani et al. constructed an electrochemical sensing platform based on Pt/Fe_3O_4/rGO, which showed excellent sensing performance towards NADH. The synergistic effect between Pt, Fe_3O_4, and rGO was believed to be the key factor for outstanding sensing performance [12].

Furthermore, the additional improvements of sensing performances can be achieved by engineering the morphology and architecture of the nanocomposites in view of increasing electrochemical active sites as well as facilitating the mass transfer [16]. Hollow porous materials are proved to be one class of preferable nanostructures with the virtues of high specific surface area, more active sites, and unlimited mass transport pathway. Based on the above considerations, porous PtAg alloy nanoshells supported on reduced graphene oxide (PtAg/rGO) were designed and prepared for the effective quantitative detection of NADH in the current work. The electron transfer rate of NADH oxidation over PtAg/rGO was significantly improved, resulting in the low working potential, the high sensitivity, and wider linear range of NADH detection. The as-constructed sensors could boost the NADH oxidation at as low as 0.15 V. The superior selectivity and long-term durability of the PtAg/rGO-based sensors provide the foundation for the practical application. The enhanced sensing performance stems from the unique architecture and specific composition of the PtAg/rGO nanocomposites. The combination of interconnected PtAg network shell and conductive rGO substrate endows the PtAg/rGO nanocomposite with distinct structure superiorities of smooth channels, rich surfaces area, alloying effect, and integral conductive matrix. Consequently, the as-obtained PtAg/rGO could provide fluent mass transport with more active sites to full contact with reaction medium during electrochemical catalysis. The dual effects of integral interconnected PtAg network backbone and conductive rGO substrate facilitates the unblocked electron transport. Impressively, the reliability of the as-developed biosensors was verified by the determination of NADH in human serum samples by standard addition method, demonstrating its promising application potential in NADH-related disease diagnostics.

Experimental

Reagents and apparatus

All reagents were of analytical grade and used as received. Chloroplatinic acid hexahydrate ($H_2PtCl_6.6H_2O$), silver nitrate ($AgNO_3$), and graphene oxide (GO) were obtained from Aladdin Industrial Inc. Uric acid (UA) and ascorbic acid (AA) were supplied by Sigma-Aldrich. 4-Acetamidophenol (AC) was purchased from Macklin. Other chemicals were obtained from Sinopharm Chemical Reagent Co. Ltd. Ultra-pure water (18.2 MΩ cm) was used throughout.

The X-ray diffraction (XRD) patterns of the samples were recorded on a Bruker D8 advanced X-ray diffractometer using Cu Kα radiation (a step rate of 0.04 s^{-1}). The microstructures of the products were acquired on a JEM-2100 transmission electron microscope. The elemental mapping images, high-resolution TEM (HRTEM), and the selected area electron diffraction (SAED) were obtained on scanning transmission electron microscopy-energy-dispersive X-ray spectroscopy (EDS) (JEM 2100F TEM equipped with a STEM unit). The laser Raman spectrometer (Raman, Horiba) was applied to get the Raman spectra. The surface elemental oxidation states of the samples were revealed by X-ray photoelectron spectrometer (XPS, PHI 5000). The thermogravimetric analysis (TGA)

was performed on the TGA/DSC1/1600HT analyzer. The Fourier transform infrared spectrum (FTIR) was observed with a Vertex 70 FTIR spectrometer (Bruker, USA) in KBr pellets. The *I-V* characteristics data were recorded on a Solartron ModuLab XM electrochemical system. A CHI 760D electrochemical workstation (Shanghai CH Instruments Co., China) was utilized to carry out all electrochemical measurements. A typical three-electrode system was employed with a glassy carbon electrode (GCE, 4 mm in diameter) as the working electrode, saturated Ag/AgCl electrode as the reference electrode, and platinum foil as the counter electrode.

Preparation of PtAg/rGO composite

The silver-ammonia solution was prepared by mixing the $AgNO_3$ and diluted $NH_3.H_2O$ (3%). After the $AgNO_3$ (200 mg) dissolved in 5 mL water, $NH_3.H_2O$ (3%) was added into the solution dropwise until the precipitate disappeared totally.

In a typical procedure, 100 mg of GO was dispersed in 50 mL H_2O followed by sonication for 1 h to make sure the full stripping of GO. Then, the fresh silver-ammonia solution was added into the GO under stirring and kept at 50 °C for 2 h. After raising the temperature to 95 °C, the glucose solution (20 mg mL^{-1}, 50 ml) was introduced to the solvent and kept at 95 °C for another 1 h. The product was washed several times with deionized water and absolute ethanol for further use.

After the vacuum drying at 60 °C for 24 h, the as-prepared product (7.2 mg) was dispersed in H_2PtCl_6 aqueous solution (2 mM, 20 ml) at 30 °C for 1 h. The final PtAg/rGO sample was obtained by etching precursor in $NH_3.H_2O$ (28%) for 15 min at room temperature and rinsed several times with water.

Preparation of the modified electrodes

One milligram PtAg/rGO powder, 1.0 mg carbon, 200 μL Nafion solution (0.5 wt.%), and 400 μL isopropanol were mixed under sonication for 30 min to form uniform catalyst ink. The working electrode was modified by dripping suitable amount of catalyst ink on a polished GCE and then dried. For reference, rGO and Ag/rGO modified electrodes were also prepared in the similar way with the same amount of catalyst added.

NADH detection in human serum

Human serum samples were stored in a refrigerator before use. The human serum was diluted 200 times by injecting 0.1 M PBS (pH 7.4). Then, the solution was spiked with known amounts of a standard NADH solution to obtain NADH concentrations of 20.0, 40.0, and 60.0 μmol L^{-1}.

Results and discussion

Choice of materials

Pt-based nanostructures have been widely applied in the electrochemical sensors because of their excellent electrocatalytic activity and biocompatibility. However, the scarce reserve of Pt, easy poisoning from intermediates, and the sluggish electron transfer kinetics limit their large-scale application. Some effective strategies, including the formation of Pt-based alloy, dispersion on conductive supports, as well as the reduction of the Pt loading, are efficient way to overcome these disadvantages [9]. Ag was selected as the secondary composition of the Pt alloy due to the following reasons. First, Ag possesses a similar lattice constant to that of Pt, which can facilitate the rational arrangement of heteroatoms in the PtAg alloy [11]. Second, the d-band center of PtAg shifts upwards compared with pure Pt. The favorable electronic structures of the PtAg catalysts will alter the chemisorption capacity towards the reactants, which is expected to improve the catalytic performance [17]. Third, the Ag atoms could improve the anti-poisoning ability and the thermodynamic stability of Pt-based catalysts [17, 18]. Segregation of Ag atoms on the PtAg alloy surface can reduce the number of neighboring Pt atoms and decrease the adsorption sites of toxic intermediate [17]. Besides, Ag has two distinct advantages, including excellent electrical conductivity and the relative low price. Porous PtAg nanoshells were fabricated in view of increasing the surface area and exposing more active sites. Moreover, graphene-based materials were chosen as the conductive support to further enhance the electrocatalytic performances of the PtAg alloy [14]. Compared with other graphene-based materials, the reduced graphene oxide has several remarkable merits of high conductivity, large specific surface area, and outstanding chemical activity. According to the above considerations, porous PtAg/rGO nanostructures have been developed as the catalysts with both high activity and stability for NADH oxidation.

Characterization of the PtAg/rGO

The TEM characterizations demonstrated that the PtAg nanoshells consist of continuous skeleton with uniform pores well distributed on the surface. Figure 1a and b present the TEM images of the Ag/rGO sample, from which the uniform spherical nanostructure with no brightness contrast were observed on the translucent nanosheet, demonstrating the solid nature of the Ag particles. The PtAg particles were well dispersed on the rGO nanosheets with the diameter mainly distributed around 20 nm (20.5 ± 4 nm, $n = 50$) (Fig. 1c–e). The obvious brightness contrast between the dark ligament shell and relatively bright center revealed the hollow nature of the PtAg nanoparticles. The well-distributed bright regions penetrating

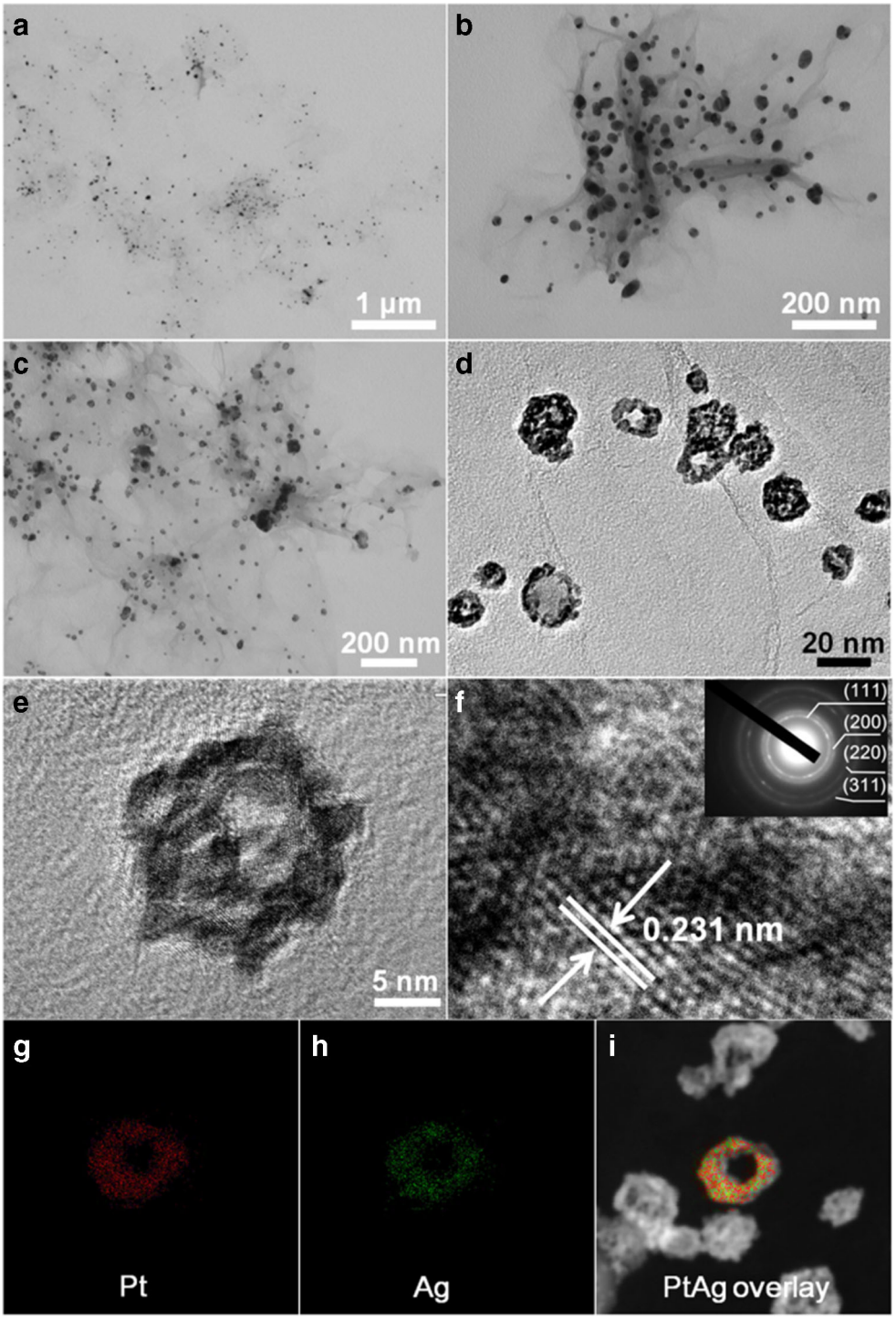

Fig. 1 TEM images of the Ag/rGO composite (**a**, **b**) and PtAg/rGO composite (**c**–**f**). The SAED image of the PtAg/rGO (the inset of Fig. 1f). Elemental mapping images of the PtAg/rGO composite (**g**–**i**)

on the dark framework in Fig. 1e indicated the formation of uniform pores throughout the PtAg nanoshells. The well-resolved ordered fringes with lattice spacing of 0.231 nm in Fig. 1f can be ascribed to the (111) plane of PtAg alloy [19]. The SAED image presents obvious diffraction rings assigned to the (111), (200), (220), and (311) facets of PtAg alloy (the inset of Fig. 1f). The elemental mappings clearly showed the uniform distribution of Pt and Ag elements throughout the entire nanostructure, demonstrating the good chemical homogeneity of PtAg alloy (Fig. 1g–i). The EDS result illustrated that its composition is $Pt_{66}Ag_{34}$ (at %) (Fig. S1). The growth mechanism of porous PtAg/rGO composite particles is illustrated in Fig. S2 [8, 10, 20].

XRD was used to examine the evolution process of crystal structures during the preparation process. XRD of the GO, rGO, and the final product are shown in Fig. 2a, which illustrates the

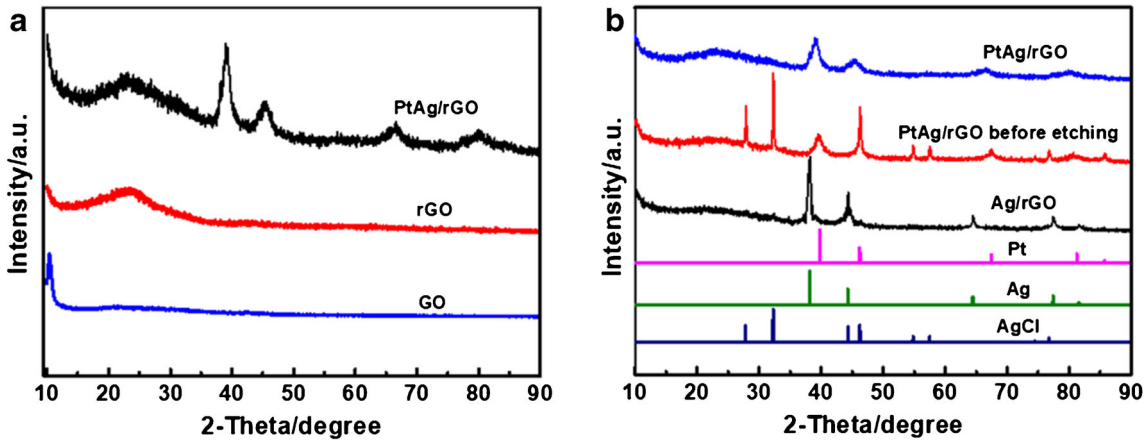

Fig. 2 XRD patterns of the resulting samples in the different preparation stages

successful formation of PtAg/rGO composites after the glucose reduction [21–23]. The detailed analysis of Fig. 2a can be seen in the electronic supporting material (Fig. S3). As depicted in Fig. 2b, all diffraction peaks of Ag/rGO can be indexed to Ag and rGO without any parasitic phases. The diffraction pattern of the resulting sample before $NH_3.H_2O$ etching testified the formation of AgCl in galvanic replacement reaction. After dissolution of AgCl in ammonia, the diffraction patterns of rGO were reserved and one set of four diffraction peaks at 38.7°, 45.3°, 65.3°, and 79.8° appear. The location of four peaks was just between standard diffraction peaks of pure Pt and Ag with no other peaks appeared, illustrating the formation of a homogeneous single-phase PtAg alloy [23]. The XRD results revealed that GO, Ag/rGO, PtAg-AgCl/rGO, and PtAg/rGO phases were involved in the synthesis process and also verified that the final product was PtAg/rGO composite.

As presented in Fig. S4, Raman spectrum was also applied to confirm the formation of rGO in the PtAg/rGO composite [24–27]. According to the TGA of the PtAg/rGO nanocomposites, the metal loading of final product is about 78 wt.% (Fig. S5) [9]. XPS of PtAg/rGO indicate that Pt^0, Ag^0, and rGO are the dominated specie of PtAg/rGO [9]. The negative shift of Pt^0 and Ag^0 binding energies declares the strong electron transfer between the conductive rGO nanosheets and the PtAg alloy (Fig. S6) [28]. The disappearance of the characteristics of oxygen-containing groups in the FTIR spectrum of PtAg/rGO also manifest the successful reduction of GO by glucose (Fig. S7) [29–31]. The *I-V* characteristics data were collected by the two point probe technique to evaluate the conductivity of PtAg/rGO. As shown in Fig. S8, the *I-V* curve exhibit Ohmic characteristic and the conductivity of PtAg/rGO is calculated to be 3.12×10^{-3} S cm^{-1}.

Electrochemical sensing of NADH over PtAg/rGO

Along with the fascinating structure features of PtAg/rGO composite, it is interesting to evaluate its electrocatalytic performance towards NADH oxidation. Figure 3 exhibits the cyclic voltammetric (CV) profiles of PtAg/rGO modified electrode in the absence/presence of 3 mM NADH in PBS (pH 7.4), with those of bare CGE, rGO, and Ag/rGO included for comparison. The current increased slightly after the addition of NADH over bare GCE, rGO, and Ag/rGO modified electrodes (Fig. 3a–c), demonstrating that no strong electrochemical responses were produced from the NADH oxidation at these electrodes. Furthermore, the oxidation peak was noted at 0.57 V on bare CGE, while no typical oxidation peaks appeared on rGO and Ag/rGO modified electrodes.

Among all these electrodes, a 4-fold increased current was observed on PtAg/rGO with the lowest oxidation potential of NADH at 0.24 V (Fig. 3d). Comparatively, the largest current response and a ca. 330 mV reduction in oxidation peak potential were obtained on PtAg/rGO modified electrode, illustrating the greatly improved NADH oxidation. It is noted that this anodic peak potential is also much lower than many reported values of NADH electrooxidation [4, 15, 32, 33]. The increase of current response and reduction of the overpotential in this work were clearly related to the improved electron transfer kinetics of NADH oxidation and the excellent electrocatalytic effect of PtAg/rGO, which is considered to originate from the high electron conductivity, abundant reactivity sites, and specific alloying effect.

The influence of the pH and the concentration of the electrocatalytic material on the sensing performance were evaluated to optimize the electrochemical test conditions. As displayed in Fig. S9a, the pH has an important impact on the electrochemical response. When the pH is less than 7.4, the electrochemical response towards 0.5 mM NADH at 0.15 V increased with the pH values. When increasing the pH value to 7.4, the PtAg/rGO-based biosensors present the best sensitivity. However, the continuous increase of the pH over 7.4 leads to the significant decrease of the sensitivity. As a result, the pH of 7.4 was chosen for the electrochemical test. The amount of the PtAg/rGO nanocomposites also affects the electrochemical response of the PtAg/rGO-based biosensors. As displayed in Fig. S9b, the electrochemical response varied with the amount of PtAg/rGO

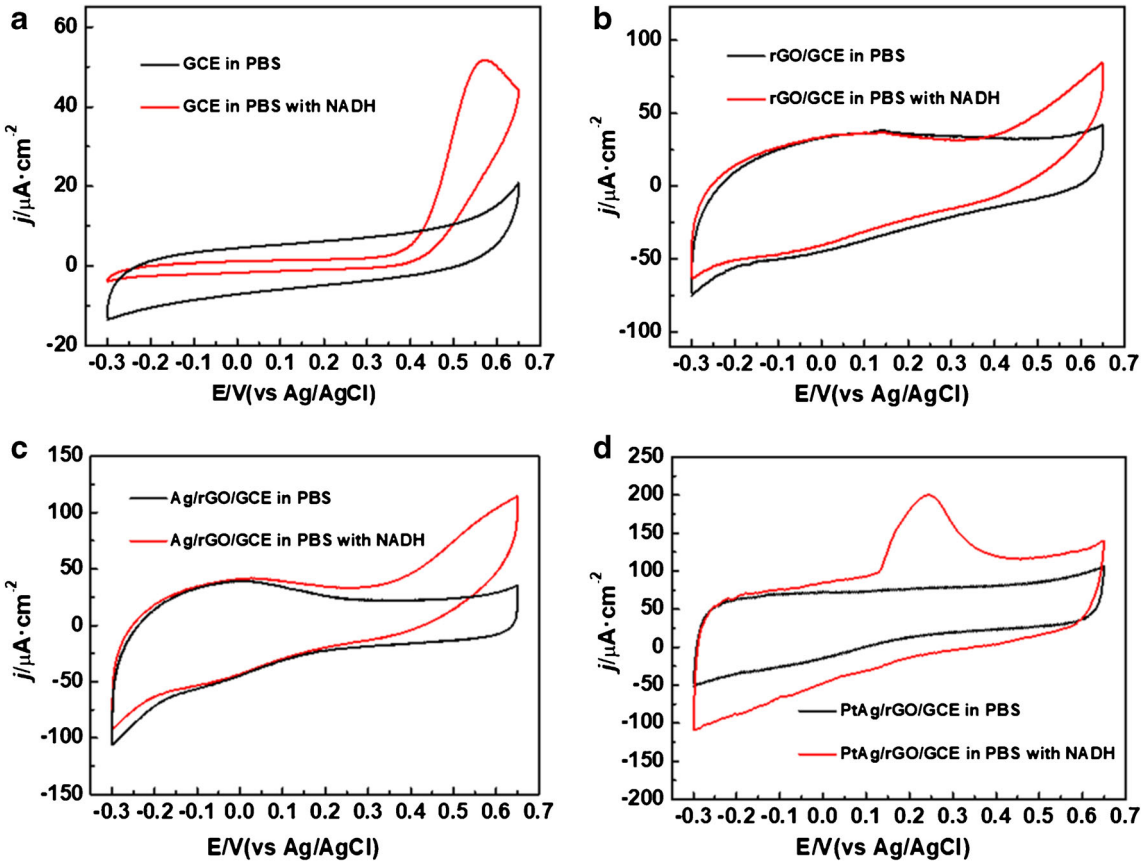

Fig. 3 CVs of different electrodes in the PBS (pH 7.4) and PBS with 3 mM NADH solution at 50 mV s^{-1}: **a** bare GCE, **b** rGO, **c** Ag/rGO, and **d** PtAg/rGO modified electrodes

nanocomposites. The electrochemical response is continuously increased when 0.3, 0.5, 0.7, 1, 1.5, 2, and 3 mg of PtAg/rGO nanocomposites are used to prepare the catalyst ink, respectively, which may result from the increased catalyst loadings. After converting the electrochemical response to current density, it is observed that the electrode modified by 0.7 mg PtAg/rGO exhibits the largest sensitivity. The electrode modified by 1.0 mg PtAg/rGO shows similar electrochemical response. However, the electrodes modified by 2.0 mg and 3.0 mg catalyst present less sensitivity, which may be due to the overlap of the active sites caused by the excess usage of the electrocatalytic material. According to these observations, 1 mg PtAg/rGO was added to 200 μL Nafion solution (0.5 wt.%) and 400 μL isopropanol to prepare the catalyst ink.

The electrocatalytic behavior of PtAg/rGO towards NADH oxidation was further explored by changing the scan rate. The CV profiles of PtAg/rGO modified electrode in the presence of 3 mM NADH in PBS (pH 7.4) at the scan rates of 25, 50, 75, 100, 125, 150 to 200 mV s^{-1} were recorded (Fig. S10a). The peak currents from the NADH oxidation gradually enhanced and the peak potential shifted positively with increasing the scan rate. The linear dependence of anodic peak currents vs. the square root of scan rate was observed with the linear equations j (μA cm^{-2}) = (20.29 ± 2.68) ( )$^{1/2}$ + 94.72 (R^2 = 0.994, n = 3) (Fig. S10b). The linear relationship suggests that the electrochemical oxidation NADH over the PtAg/rGO is controlled by the diffusion of electroactive species [34].

The amperometric response upon the successive additions of NADH in PBS was carried out at 0.15 V to evaluate the sensitivity of PtAg/rGO-based biosensors. As Fig. 4a illustrates, after the addition of NADH, the oxidation current increased immediately and approached the maximum steady-state current within 3 s. Moreover, the response currents on PtAg/rGO are proportional to the concentration of NADH in the concentration range from 2.0 to 2378 μM, the linear regression equations is j (μA cm^{-2}) = (92.62 ± 5.87) [NADH] (mM) + 2.43, R^2 = 0.991 (n = 3) with a high sensitivity of (92.62 ± 5.87) μA mM^{-1} cm^{-2} (Fig. 4b). The detection limit is estimated to be 0.2 μM (S/N = 3).

The selectivity, reproducibility, and durability for NADH detection over PtAg/rGO

The selectivity, reproducibility, and durability of the as-constructed PtAg/rGO biosensor were also carried out to evaluate its sensing performance. As shown in Fig. 5a, the interference effect of 5 mM AA, 5 mM AC, 5 mM UA, 5 mM glucose and 5 mM H_2O_2, on current response of NADH over

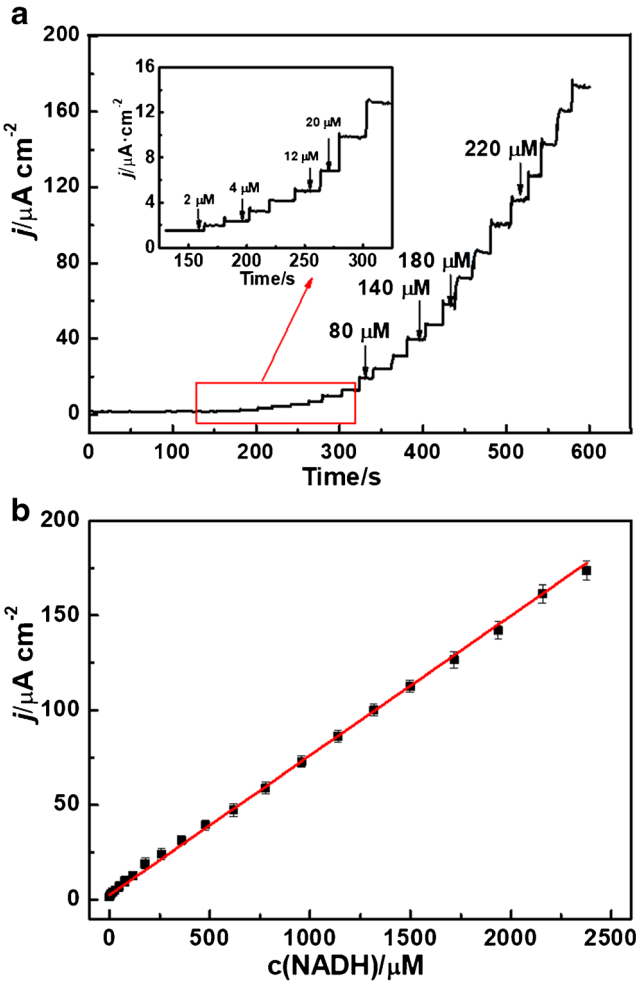

Fig. 4 **a** Amperometric current responses of the PtAg/rGO modified electrode on successive addition of NADH into stirring PBS (pH 7.4) at 0.15 V. **b** Calibration plot of amperometric response vs. different NADH concentrations at 0.15 V

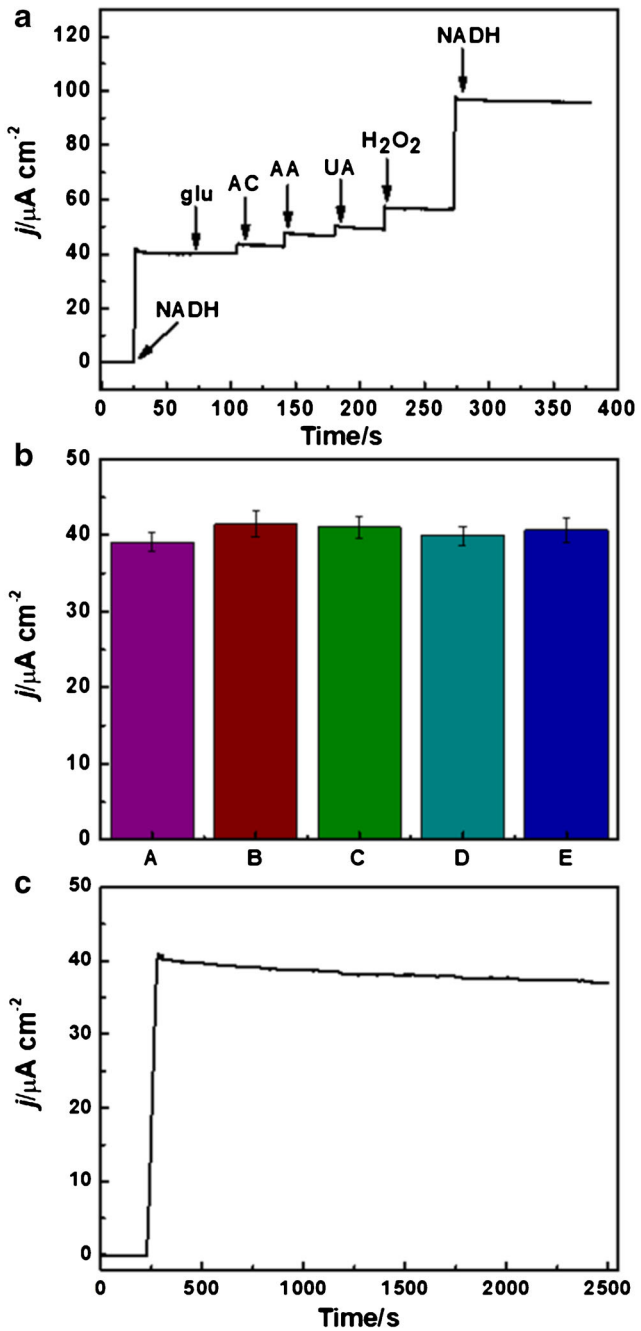

Fig. 5 **a** Amperometric responses to the successive addition of 0.5 mM NADH, 5 mM glucose, 5 mM AC, 5 mM AA, 5 mM UA, 5 mM H_2O_2, and 0.5 mM NADH in 0.1 M PBS (pH 7.4) at 0.15 V. **b** Column graph of current responses of five PtAg/rGO modified electrodes in 0.1 M PBS (pH 7.4) with 0.5 mM NADH at 0.15 V. **c** Amperometric currents of PtAg/rGO in a stirring PBS (pH 7.4) with 0.5 mM NADH for 2500 s at 0.15 V

PtAg/rGO, was monitored. The acceptable tiny electrochemical signals from the typical interferents indicate the good selectivity of the as-constructed sensing devices. The reproducibility of sensors was estimated by comparing the current responses of five different electrodes towards 0.5 mM NADH at 0.15 V under the same condition. The averaged current responses is (40.45 ± 1.32) μA cm^{-2} ($n = 5$) (Fig. 5b), demonstrating the good reproducibility of the developed sensors. One of the advantages of the PtAg/rGO-based sensor for NADH detection is its highly long-term catalytic durability, which is performed by testing the steady-state activity using potentiostatic method. As displayed in Fig. 5c, a stable amperometric response can be observed with 0.5 mM NADH in stirring PBS after continuously running for 2500 s under 0.15 V, indicating the high capability of long-term NADH detection over PtAg/rGO. Besides, the resistance to the fouling of the sensors has also been tested. As shown in Fig. S11, the amperometric responses of PtAg/rGO modified electrodes towards 0.5 mM NADH at 0.15 V was tested once a day. The current density did not exhibit obvious change over 30 days, which illustrates that the PtAg/rGO modified electrodes have strong resistance to the fouling.

A comparison of the sensing performances of the PtAg/rGO modified electrode with the previously reported NADH sensors is shown in Table S1 [4, 15, 32, 33, 35]. Compared

with the previous methods, the as-constructed sensors could realize the NADH oxidation at the low working potential of 0.15 V without the aid of redox mediators and enzyme. The electron-transfer kinetics of NADH oxidation over PtAg/rGO was greatly optimized, which promotes the low working potential, the high sensitivity, and wider linear range of NADH detection. The outstanding selectivity, continuous durability test over 2500 s, and excellent resistance to the fouling over 30 days of the sensors provides the precondition for the NADH detection in the real sample. Such intriguing sensing performances result from the unique hollow nanoporous architecture, specific alloying effect, and the integral conductive matrix. The continuous PtAg network shell and the effective synergistic effect between PtAg alloy and rGO benefit the rapid electron transfer during electrochemical oxidation of NADH. The open channels and rich voids of hollow porous structure provide unlocked mass transport route to reduce the response time. Additionally, the large surface area from the inner and outer surfaces supplies abundant active sites to improve the sensing sensitivity.

Detection of NADH in human serum samples

To investigate the practical applicability of the PtAg/rGO biosensors for the NADH determination, standard addition method was carried out to determinate NADH concentrations in human serum spiked PBS. The serum samples were diluted 200 times with 0.1 M PBS before measurement without any other pretreatment. As shown in Table S2, a satisfactory result was obtained with high recovery of NADH in the range of 96.5–97.0% and low RSD values of 3.7–4.5%. Herein, the as-developed biosensor presents the respectable reliability and applicability for determination of NADH in human serum samples.

Conclusions

Porous PtAg nanoshells supported on reduced graphene oxide with interconnected skeleton and narrow pore distribution were successfully fabricated through the facile one-step reduction of $[Ag(NH_3)_2]^+$ and GO, followed by the spontaneous galvanic replacement reaction. The specific architecture and the synergistic catalytic effect endow the PtAg/rGO nanocomposite with superior electrocatalytic activity towards NADH oxidation without any enzyme and redox mediator. Importantly, the proposed biosensors based on PtAg/rGO showed extraordinary sensing performances towards NADH detection, exhibiting low applied potentials, high sensitivity, outstanding selectivity, wide linear range, and excellent long-time durability. Inspiringly, the accurate detection of NADH in human serum samples with good recovery was well accomplished over the as-constructed biosensors. The original strategy described in current work not only provides superior biosensors for NADH detection but also manifests the PtAg/rGO as the great candidate in other fields with the advantages of fast mass and electron transport, high surface area, and unique structure stability.

In our opinion, the future direction of the electrochemical NADH detection may continuously focus on the reduction of the working overpotential and improvement of the electron transfer kinetics. More sensors that realize the nanomolar levels or even less of NADH measurement at much lower potentials are required to be developed. Besides, the nanomaterials with high biocompatibility are also encouraged on the purpose of application in the bioassay.

Funding This work was supported by the National Natural Science Foundation of China (51772133), and Natural Science Foundation of Shandong Province (ZR2017JL022), and the project of "20 items of University" of Jinan (2018GXRC001) and Case-by-Case Project for Top Outstanding Talents of Jinan.

Compliance with ethical standards

Conflict of interest The authors declare that they have no conflicts of interest.

References

1. Baradoke A, Pastoriza-Santos I, González-Romero E (2019) Screen-printed GPH electrode modified with Ru nanoplates and PoPD polymer film for NADH sensing: design and characterization. Electrochim Acta 300:316–323
2. Shetti NP, Bukkitgar SD, Reddy KR, Reddy Ch V, Aminabhavi TM (2019) ZnO-based nanostructured electrodes for electrochemical sensors and biosensors in biomedical applications. Biosens Bioelectron 141:111417
3. Selvarani K, Prabhakaran A, Arumugam P, Berchmans S, Nayak P (2018) 2D $MoSe_2$ sheets embedded over a high surface graphene hybrid for the amperometric detection of NADH. Microchim Acta 185:411 (8 pp)
4. Liu X, Li B, Ma M, Zhan G, Liu C, Li C (2012) Amperometric sensing of NADH and ethanol using a hybrid film electrode modified with electrochemically fabricated zirconia nanotubes and poly (acid fuchsin). Microchim Acta 176:123–129
5. Liu X, Li B, Wang X, Li C (2010) One-step construction of an electrode modified with electrodeposited Au/SiO_2 nanoparticles, and its application to the determination of NADH and ethanol. Microchim Acta 171:399–405
6. Cui L, Ai S, Shang K, Meng X, Wang C (2011) Electrochemical determination of NADH using a glassy carbon electrode modified with Fe_3O_4 nanoparticles and poly-2,6-pyridinedicarboxylic acid, and its application to the determination of antioxidant capacity. Microchim Acta 174:31–39
7. Tığ GA (2017) Highly sensitive amperometric biosensor for determination of NADH and ethanol based on Au-Ag nanoparticles/poly(L-cysteine)/reduced graphene oxide nanocomposite. Talanta 175:382–389
8. Xu H, Yan B, Li S, Wang J, Wang C, Guo J, du Y (2018) Facile construction of N-doped graphene supported hollow PtAg nanodendrites as highly efficient electrocatalysts toward formic acid oxidation reaction. ACS Sustain Chem Eng 6:609–617

9. Lv J, Feng J, Li S, Wang Y, Wang A et al (2014) Ionic liquid crystal-assisted synthesis of PtAg nanoflowers on reduced graphene oxide and their enhanced electrocatalytic activity toward oxygen reduction reaction. Electrochim Acta 133:407–413
10. Hong X, Tan C, Liu J, Yang J, Wu X et al (2015) AuAg nanosheets assembled from ultrathin AuAg nanowires. J Am Chem Soc 137: 1444–1447
11. Li Z, Li Y, He C, Shen PK (2017) Bimetallic PtAg alloyed nanoparticles and 3-D mesoporous graphene nanosheet hybrid architectures for advanced oxygen reduction reaction electrocatalysts. J Mater Chem A 5:23158–23169
12. Roushani M, Hoseini SJ, Azadpour M, Heidari V, Bahrami M, Maddahfar M (2016) Electrocatalytic oxidation behavior of NADH at Pt/Fe_3O_4/reduced-graphene oxide nanohybrids modified glassy carbon electrode and its determination. Mater Sci Eng C 67: 237–246
13. Haque E, Yamauchi Y, Malgras V, Reddy KR, Yi JW, Hossain Md Sr A, Kim J (2018) Nanoarchitectured graphene-organic frameworks (GOFs): synthetic strategies, properties, and applications. Chem Asian J 13:3561–3574
14. Xu J, Wang Y, Hu S (2017) Nanocomposites of graphene and graphene oxides: synthesis, molecular functionalization and application in electrochemical sensors and biosensors. A review. Microchim Acta 184:1–44
15. Govindhan M, Amiri M, Chen A (2015) Au nanoparticle/graphene nanocomposite as a platform for the sensitive detection of NADH in human urine. Biosens Bioelectron 66:474–480
16. Sadeghian RB, Han J, Ostrovidov S, Salehi S, Bahraminejad B et al (2017) Macroporous mesh of nanoporous gold in electrochemical monitoring of superoxide release from skeletal muscle cells. Biosens Bioelectron 88:41–47
17. Peng Z, You H, Yang H (2010) An electrochemical approach to PtAg alloy nanostructures rich in Pt at the surface. Adv Funct Mater 20:3734–3741
18. Ramirez-Caballero GE, Ma Y, Callejas-Tovar R, Balbuena PB (2010) Surface segregation and stability of core–shell alloy catalysts for oxygenreduction in acid medium. Phys Chem Chem Phys 12:2209–2218
19. Li J, Rong H, Tong X, Wang P, Chen T, Wang Z (2018) Platinum-silver alloyed octahedral nanocrystals as electrocatalyst for methanol oxidation reaction. J Colloid Interface Sci 513:251–257
20. Topsakal M, Ciraci S (2011) Static charging of graphene and graphite slabs. Appl Phys Lett 98:131908 (4pp)
21. Hao J, Ji L, Wu K, Yang N (2018) Electrochemistry of ZnO@reduced graphene oxides. Carbon 130:480–486
22. Zhu C, Guo S, Fang Y, Dong S (2010) Reducing sugar: new functional molecules for the green synthesis of graphene nanosheets. ACS Nano 4:2429–2437
23. Cao X, Wang N, Han Y, Gao C, Xu Y, Li M, Shao Y (2015) PtAg bimetallic nanowires: facile synthesis and their use as excellent electrocatalysts toward low-cost fuel cells. Nano Energy 12:105–114
24. Zhou G, Wang D, Li F, Zhang L, Li N et al (2010) Graphene-wrapped Fe_3O_4 anode material with improved reversible capacity and cyclic stability for lithium ion batteries. Chem Mater 22:5306–5313
25. Dong Y, Ma R, Hu M, Cheng H, Yang Q, Li YY, Zapien JA (2013) Thermal evaporation-induced anhydrous synthesis of Fe_3O_4-graphene composite with enhanced rate performance and cyclic stability for lithium ion batteries. Phys Chem Chem Phys 15: 7174–7181
26. Ye J, Hao Q, Liu B, Li Y, Xu C (2017) Facile preparation of graphene nanosheets encapsulated Fe_3O_4 octahedra composite and its high lithium storage performances. Chem Eng J 315:115–123
27. Yousaf AB, Muhammad I, Zeb A, Wen T, Xie X, Jiang Y, Yuan C, Xu A (2016) Single phase PtAg bimetallic alloy nanoparticles highly dispersed on reduced graphene oxide for electrocatalytic application of methanol oxidation reaction. Electrochim Acta 197:117–125
28. Lopez V, Sundaram RS, Gomez-Navarro C, Olea D, Burghard M, Gomez-Herrero J et al (2009) Chemical vapor deposition repair of graphene oxide: a route to highly-conductive graphene monolayers. Adv Mater 21:4683–4686
29. Layek RK, Uddin E, Kim NH, Lau AKT, Lee JH (2017) Noncovalent functionalization of reduced graphene oxide with pluronic F127 and its nanocomposites with gum arabic. Compos Part B 128:155–163
30. Cheng J, Chen Y, Yeh Y, Hy S, Kuo L, Hwang B (2016) Enhancement of electrochemical properties by freeze-dried graphene oxide via glucose-assisted reduction. Electrochim Acta 197:146–151
31. Hu Y, Liu Z, Xu J, Huang Y, Song Y (2013) Evidence of pressure enhanced CO_2 storage in ZIF-8 probed by FTIR spectroscopy. J Am Chem Soc 135:9287–9290
32. Mutyala S, Mathiyarasu J (2016) A highly sensitive NADH biosensor using nitrogen doped graphene modified electrodes. J Electroanal Chem 775:329–336
33. Wang Q, Li W, Bao N, Yu C, Gu H (2016) Low-potential amperometric determination of NADH using a disposable indium-tin-oxide electrode modified with carbon nanotubes. Microchim Acta 183:423–438
34. Hajian R, Yusof NA, Faragi T, Shams N (2014) Fabrication of an electrochemical sensor based on gold nanoparticles/carbon nanotubes as nanocomposite materials: determination of myricetin in some drinks. PLoS One 9:1–7
35. Roushani M, Karami M, Dizajdizi BZ (2017) Amperometric NADH sensor based on a carbon ceramic electrode modified with the natural carotenoid crocin and multi-walled carbon nanotubes. Microchim Acta 184:473–481